Science of the Total Environment 900 (2023) 166404

Contents lists available at ScienceDirect

Science of the Total Environment

journal homepage: www.elsevier.com/locate/scitotenv

Application of two-dimension, high-resolution evidences to reveal the biogeochemical process patterns of trace metals in reservoir sediments

Quan Chen [a,b], Shu Xu [a], Jingfu Wang [a,b,*], Dengjun Wang [c], Zhihui Dai [d], Peng Liao [a,b], JiaoJiao Yang [a,b], Wen Guo [a,b], Shiming Ding [b,e], Jingan Chen [a,b,*]

[a] State Key Laboratory of Environmental Geochemistry, Institute of Geochemistry, Chinese Academy of Sciences, Guiyang 550081, PR China
[b] University of Chinese Academy of Sciences, Beijing 100049, PR China
[c] School of Fisheries, Aquaculture and Aquatic Sciences, Auburn University, Auburn, AL 36849, USA.
[d] State Key Laboratory of Ore Deposit Geochemistry, Institute of Geochemistry, Chinese Academy of Sciences, Guiyang 550081, PR China
[e] State Key Laboratory of Lake Science and Environment, Nanjing Institute of Geography and Limnology, Chinese Academy of Sciences, Nanjing 210008, PR China

HIGHLIGHTS

- 2D-HR distributions of TMs in sediments were determined by LA-ICP-MS.
- Distributions within microniches in horizontal reflect mobilization of TMs.
- Vertical distributions record the diagenesis of TMs in sedimentation.
- 2D-HR data broad the understanding to the biogeochemical processes of TMs.

GRAPHICAL ABSTRACT

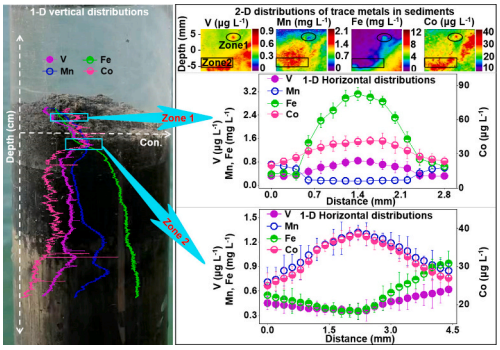

ARTICLE INFO

Editor: Daniel CW Tsang

Keywords:
Trace metals
2D-HR evidences
Mobilization
Diagenesis
Reservoir sediments

ABSTRACT

Pollutions of trace metals (TMs) in reservoirs are blooming due to TMs were trapped efficiently in reservoir sediments by dams. Despite the mobilization of TMs in sediments have been well-documented, the patterns of biogeochemical processes occurred in sediments remain poorly understanding. Herein, a deep reservoir was selected to investigate the patterns of TMs biogeochemical processes in sediments by using high-resolution ZrO-Chelex-AgI diffusive gradient in thin films technique (HR-ZCA DGT) and the laser ablation inductively coupled plasma mass spectrometry (LA-ICP-MS). 2-dimension high-resolution (2D-HR) images showed significant differential spatial enrichment of TMs (V, Mn, Fe, Co, Zn and Sb) in sediments, indicating strong heterogeneity in sediments. Correlations of TMs within microniches (diameter < 1 mm) in horizontal were usually different even contrast with that in vertical profile, suggesting distinct biogeochemical process patterns occurred in vertical vs. in horizontal. Further analyses from 2D-HR images showed the distributions of TMs in microniches reflected their mobilization that was driven by microenvironmental conditions. In contrast, distributions in sediment vertical profile recorded the diagenesis in different deposition depth. The diagenesis in sediment vertical is

* Corresponding authors at: State Key Laboratory of Environmental Geochemistry, Institute of Geochemistry, Chinese Academy of Sciences, Guiyang, 550081, PR China.
E-mail addresses: wangjingfu@vip.skleg.cn (J. Wang), chenjingan@vip.skleg.cn (J. Chen).

https://doi.org/10.1016/j.scitotenv.2023.166404
Received 14 June 2023; Received in revised form 16 August 2023; Accepted 16 August 2023
Available online 18 August 2023

continuously accumulated by the discrete, microniches mobilization of TMs in horizontal. Collectively, our findings evidenced that 2D-HR data is an update complement to 1-dimension data for better interpret the biogeochemical process patterns of TMs in sediments, that have implication for water management to metals pollution in reservoir ecosystems.

1. Introduction

Trace metals (TMs) pollutions are blooming in freshwater sediments ecosystems globally. The number of dams has been expanded rapidly during the latest century due to the expanded need of energy production to fuel economy (Maavara et al., 2020; Rodriguez et al., 2020; Zhu et al., 2020). Almost two-thirds of the world's long rivers (>1000 km) were no longer free-flowing due to the blooming of dam construction (Grill et al., 2019; Maavara et al., 2020). These dams caused the increase of hydraulic residence time (HRT) that could facilitate the sedimentation of TMs in reservoir sediments by primary productivity, adsorption, sedimentation, or retention (Liu et al., 2020; Rodriguez et al., 2020; Zhu et al., 2020). With the operation of reservoirs, TMs trapped in sediments maybe be buried permanently during the diagenesis (Hamilton-Taylor et al., 2005; Shaw et al., 1990; Tessier et al., 1996). Alternatively, TMs could be remobilized by series biogeochemical processes occurred in sediments (Schroth et al., 2015; Shaw et al., 1990), resulting in severe TMs pollutions after TMs were diffused back into overlying water (Gao et al., 2016; Luders et al., 2020). As such, understanding the biogeochemical processes of TMs in sediments is important for evaluating the TMs pollutions in reservoir ecosystems (Liu et al., 2020).

Biogeochemical processes of TMs were usually illuminated by the interpretation of distributions and correlations along sediment vertical profile (Hamilton-Taylor et al., 2005; Och et al., 2012; Shaw et al., 1990; Tessier et al., 1996; Wang et al., 2015). However, bias even misinterpretations maybe be brought if those interpretations were solely relied on vertical profile data (Zhang et al., 2014). This is mainly as isolate vertical profile data is not sufficient for a precise interpretation on the fate and transport of TMs in the 3-dimensional space of sediments (Davison, 1993; Hamilton-Taylor et al., 2005; Stockdale et al., 2009; Zhu et al., 2006). Furthermore, vertical profile data is mainly obtained from traditional ex-situ sampling procedures that routinely including: i) collecting sediment cores, ii) slicing the sediment at a specifical vertical intervals (usually >1 cm), and iii) finally analyzing both solid and liquid phases (Stockdale et al., 2009; Zhou et al., 2020). Obviously, the low-resolution data from those ex-situ sampling cannot be used to decipher the accurate fate of TMs within small-scale (mm to μm) due to significant heterogeneity is widespread in sediments (Ding et al., 2016; Stockdale et al., 2009; Tankere-Muller et al., 2007; Zhou et al., 2020). Also, local destroys to physicochemical properties of sediment samples were inevitable during the processes of core slicing, transportation, storage, and the determination of samples (Chen et al., 2018; Stockdale et al., 2009). So, a gap was usually existed between the results determined from ex-situ sampling and the truly results in sediments. Thus, in-situ and 2-dimension data is needed to provide a comprehensive understanding to the biogeochemical processes of TMs with a fine scale in sediments.

The biogeochemical processes of TMs in sediment were well-investigated with the development and optimization of sampling techniques (Hammond et al., 2023; Xue et al., 2022; Zhu et al., 2019). Because accurate data could be determined by those advanced techniques [e.g., microelectrodes (Luther et al., 1998), planar optodes (PO) (Li et al., 2019), and the diffusive gradients in thin films technique (DGT) (Davison and Zhang, 1994; Ernstberger et al., 2002)] due to their negligible disturbance to samples during sampling (Peijnenburg et al., 2014; Stockdale et al., 2009). Biogeochemical processes of TMs deciphered by those advance techniques including: 1) mobilization during localized decomposition of organic matters (OM) (Bao et al., 2021; Fan et al., 2019; LaRowe et al., 2020), 2) desorption, reduction, and dissolution of iron (Fe) and/or manganese (Mn) (oxy)hydroxides (Bao et al., 2021; Fan et al., 2019; Tessier et al., 1996), 3) microbial metabolism (e.g., assimilation, fecal pellets, and death) (LaRowe et al., 2020; van de Velde et al., 2016), and 4) dissolution of acid-sensitive metal sulfides or carbonates (Malkin et al., 2014; van de Velde et al., 2016). In those studies, attentions were primarily paid on the mobilization mechanism of TMs in sediments. However, the underlying patterns in the occurrence of these biogeochemical processes, in particular explain how the distribution of TMs are associated with which biogeochemical process patterns in sediments by the comparison of 1D and 2D data remain unclear.

To investigate the underlying patterns of TMs biogeochemical processes in sediments, here we selected a deep reservoir (Hongfeng reservoir) which located in southwest China as the study site. The pollutions of TMs [e.g., vanadium (V), cobalt (Co), zinc (Zn) and antimony (Sb)] in Hongfeng reservoir sediments threat the health of its overlying water (Chen et al., 2019; Wang et al., 2015). Moreover, the biogeochemical processes of TMs in sediments were usually influenced by the redox of Fe and/or Mn (Bao et al., 2021; Davison, 1993). Herein, we use a novel DGT technique to sample TMs in natural sediment cores, then generate 2D-HR images through the data determined by the laser ablation inductively coupled plasma mass spectrometry (LA-ICP-MS). More specifically, we 1) tested the 2D distributions of dissolved TMs in sediments; 2) derived 1D data from a weighted average of the 2D data in sediments; and 3) analyzed the couple mobilization behavior between TMs in sediments. These results provide new insights into the biogeochemical process patterns of TMs in reservoir sediments.

2. Materials and methods

2.1. Sampling site description and sediment cores collection

Hongfeng reservoir (HF) locates in southwest of China (26°23′-26°41′ N, 106°33′-106°47′ E; Fig. 1), where is one of three regions enriched in reservoir in the word (Chen et al., 2018). HF was constructed in 1960s (mean and max depth is 11 and 45 m, respectively), and is serving as the most important drinking water sources for Guiyang city, the capital of Guizhou Province. With the rapid development of economy and the increase of population, a large amount of nutrients from HF watershed was input into the sediments of HF then facilitated HF grown to be a seasonal hypoxic reservoir (Chen et al., 2019). Moreover, a blooming TMs pollution due to industrial/agriculture wastewater was continuously discharged into HF (Wang et al., 2015). Our sampling site was located at the dam zone because it's the only outlet of the HF and reflects the level of pollution in the whole reservoir.

A gravity core apparatus with plexiglass coring tubes (length × diameter = 50 cm × 12 cm) was used to collect intact duplicate sediment cores in January (winter) and July (summer) in 2021, with a 10–20 cm depth of overlying water layer in sediment cores. After the cores were collected, a rubber stopper was used to block the bottom of cores and the DGT probe was inserted into sediments immediately. Then, the sediment cores were fixed in a self-developed tripod lander. Followed by putting the tripod lander back to the bottom of the reservoir with a nylon rope. The exposure time of cores in air was controlled to be <10 min to minimize the physiochemical disturbance for sediment cores, ensuring that the DGT probe could sample the TMs in a real in-situ condition.

2.2. Preparation, deployment, and retrieval of DGT probes

A novelty DGT device (high-resolution ZrO-Chelex-AgI DGT: HR-ZCA DGT) was selected to sample TMs in sediments (Ren et al., 2021), which is a flat-typed DGT device composed by binding gel (0.4 mm), agarose diffusion gel (0.8 mm), and a Durapore® PVDF membrane (0.10 mm thickness and 0.45 μm pore size; Millipore, USA) (Wang et al., 2017). A window (length × width = 15.0 cm × 1.8 cm) within HR-ZCA DGT probe was exposed in porewater to offer an aisle for aqueous ions of TMs and sulfides, those ions can be freely trapped by binding gel after across the diffusion layer from the window zone (Ding et al., 2016; Wang et al., 2017). HR-ZCA DGT was prepared according to the method reported in our previous work (Ren et al., 2021). After the sediment cores were collected, the HR-ZCA DGT probe was vertically inserted into sediment core manually. A 3–5 cm length of DGT gel was remained in overlying water to sample TMs and sulfides. The insert processes were operated as gentle as possible to minimize any physical disturbances to the sediment-water interfaces (SWI). Then, the cores were put back to the bottom of reservoir which located at the sample site to ensure HR-ZCA DGT probe worked within nature environment conditions. The deployment time of HR-ZCA DGT in field was maintained for 24 h to ensure that the enriched mass of TMs and sulfides could cover the lowest detection limit of the instrument. After sediment cores were retrieved in next day, soil absorbed on the probe surface was cleaned off with deionized water (DW) (resistivity: 18.2 MΩ cm). Followed by wrap the cleaned probe in aluminum foil, added a few drops of DW to keep a moisturize environment and taken the probe back to the laboratory for chemical analysis.

2.3. Treatment and analyses of HR-ZCA DGT

In laboratory, the binding gel of HR-ZCA DGT from the window zone was cut using a ceramic knife and taken out for following analyses. Firstly, the binding gel was dried as the procedures described in our previous work (Ren et al., 2021). Briefly, the binding gel was placed on three-layers clean PVDF membranes and covered by one-layer PVDF membrane. Then, the DGT gel was transferred into a gel vacuum dryer (NZG-A, JUNYI Electrophoresis, China) and dried at 50 °C for 3 h. After been dried, the central zone of the binding gel with a depth ranging from 1.0 to −3.5 cm (the depth of SWI was set as 0 cm) was mounted onto a glass microscope slides using double-sided adhesive tape, avoid uneven surface caused by air bubbles and was then further ablated (Ren et al., 2021). A blank HR-ZCA DGT gel was dried and detected with sampled gel simultaneously, and its assay value was subtracted for calculating the final concentration.

LA-ICP-MS was used to determine the concentrations of TMs [V(V), Mn(II), Fe(II), Co(II), Zn(II) and Sb(V)] and sulfide [S(II-)] in HR-ZCA DGT gel (Fig. S1). The feasibility of LA-ICP-MS as a quantitative analytical technique was tested in our previous work (Ren et al., 2021) followed the method reported by Gao et al. (2015). In short, calibration standards were prepared by plotting standardized laser ablation signals of elements (signals of elements divided by signals of internal standard ^{13}C) versus the corresponding elemental mass accumulated on the binding gel per analyzed ablation spot (pg/spot) (Gao et al., 2015). The mass of multiple elements accumulated on the binding gels per analyzed ablation spot (pg/spot) was calculated as the method described by Gao et al. (2015). Besides, the validation of HR-ZCA DGT device was conducted in our previous work by examining the relationship between the masses of TMs accumulated in HR-ZCA gel and deployment time (Ren et al., 2021), the experimental data agreed well with the theoretical predicted values (with a measured/predicted ratio for TMs between 0.99 and 1.02) validated the use of the HR-ZCA gel for DGT measurement.

An ASI RESOLution-LR-S155 laser microprobe equipped with a Coherent Compex-Pro 193 nm ArF excimer laser was used for laser sampling, with ion-signal intensities obtained using an Agilent 7700× ICP-MS instrument. To improve analytical precision, the ^{13}C, which is the major elemental component of the matrix of the binding gel, was used as an internal normalization standard as proposed by Lehto et al. (2012). The operated conditions for LA and ICP-MS analysis were summarized in Table S1. Finally, the iolite software (version 4) was used to process the data of TMs and sulfides, and to generate 2D-HR images. 1D vertical (horizontal) data came from the average of 2D-HR images data from selected zone in horizontal (vertical).

3. Results

3.1. Distributions of dissolved TMs and sulfide along sediment profiles

Significant spatial heterogeneity of TMs in sediments were evidenced by in-situ, 2D-HR images from LA-ICP-MS determinations (Fig. 2). During winter, the O_2 concentration of overlying water was usually higher than 4 mg L^{-1} indicating that overlying water was exposed in aerobic conditions (Fig. S2). In the depth range from 0.5 cm above the SWI and 3.2 cm below the SWI, V, Mn, and Zn exhibited the first distribution pattern in 1D vertical profile with two concentration peaks at the depth of −0.3 cm and − 2.7 cm, respectively (Fig. 2B, C, F). The

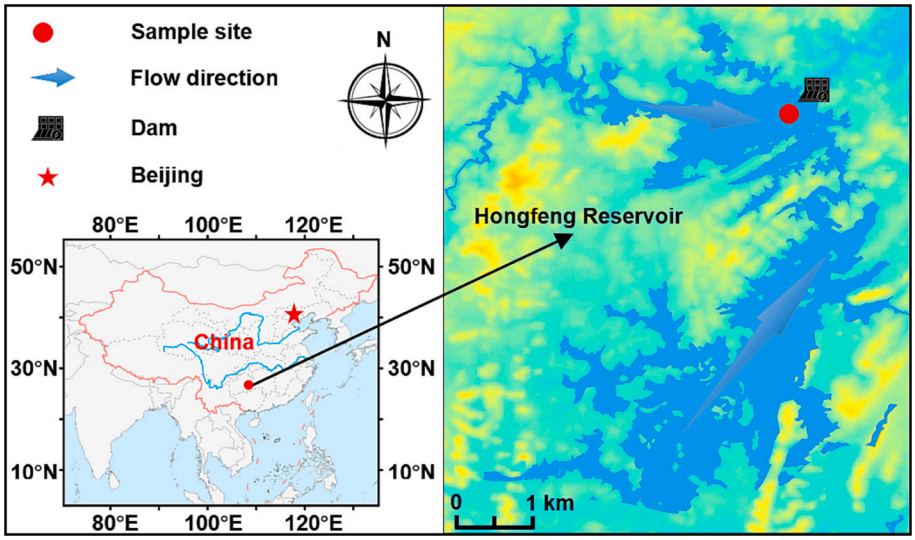

Fig. 1. The location of studying area and sampling site.

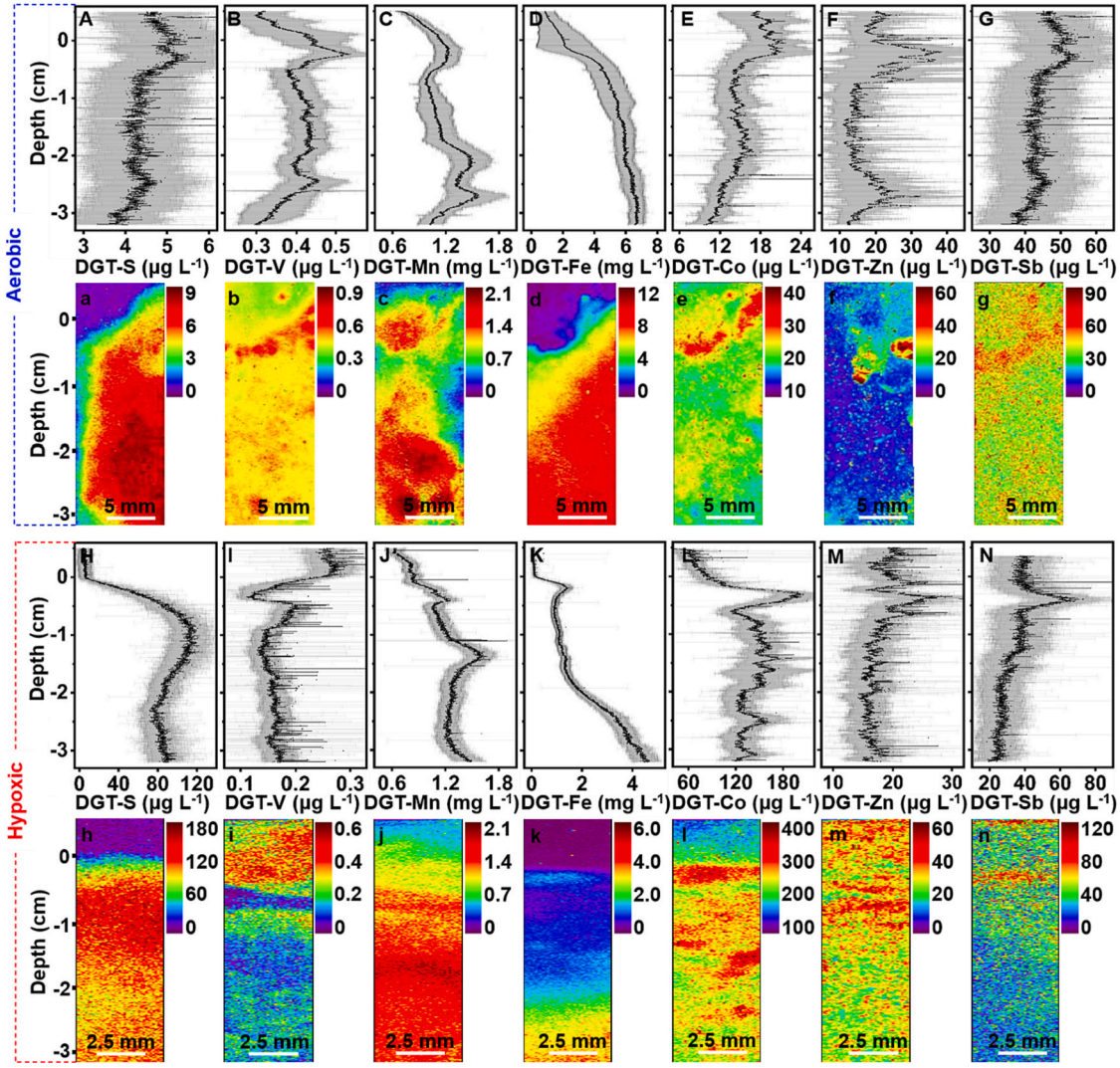

Fig. 2. Distributions of dissolved metals and dissolved sulfide in surface sediments (0.5 to − 3.2 cm depth). The 1D vertical profiles data were collected from horizontally averaged 2D images; black points and adjacent grey zones represent the mean values and standard deviations, respectively. A–G and a–g represents 1D vertical profiles and 2D-HR images, respectively, during aerobic conditions. H—N and h–n represents 1D vertical profiles and 2D-HR images, respectively, during hypoxic conditions. The depth at the sediment-water interface (SWI) was artificially set as 0 cm, positive above the SWI and negative below the SWI.

distribution pattern of sulfide was similar with that of V, Mn, and Zn (Fig. 2A). The concentrations of S, V, Mn, and Zn at −0.3 cm was 5.32 μg L^{-1}, 0.54 μg L^{-1}, 1.24 mg L^{-1}, and 39.11 μg L^{-1}, respectively. And that at −2.7 cm was 4.82 μg L^{-1}, 0.47 μg L^{-1}, 1.58 mg L^{-1}, and 32.33 μg L^{-1}, respectively. Co and Sb showed the second distribution pattern with a concentration peak at around −0.3 cm that was 19.43 μg L^{-1} and 54.62 μg L^{-1}, respectively (Fig. 2E, G). The distribution pattern of Fe was distinctly different with those above two patterns (Fig. 2D), with continuous increasing from overlying water to the sediments. Consistent with 1D vertical distributions, 2D-HR images showed that TMs were more enriched at the depth where 1D concentration peaked (Fig. 2a-g). In contrast, the 2D-HR images showed that there were significant horizontal gradients which cannot detected from the vertical 1D profiles. In vertical depth range of 0.2 to −0.5 cm around the SWI, Mn and Co were enriched on the left side in 2D-HR image, while S, V, Fe, and Zn were more concentrated on the right side, and Sb was more homogeneously distributed (Fig. 2a-g). In deeper sediments (−0.5 to −3.2 cm), S and Fe were more enriched in the right region in the 2D-HR images, Mn was elevated in the left region, while V, Co, Zn and Sb were enriched uniform.

Consistently, significant spatial heterogeneity of TMs in sediments were also observed during summer with a hypoxic condition (Fig. S2, Fig. 2H-N and h-n). Three distinct distribution patterns of TMs were also observed in 1D vertical profiles (Fig. 2H-N). Concentrations of V were higher in overlying water and declined steeply across the SWI and then remained steady in deeper sediments (Fig. 2I). Concentrations of Co, Zn and Sb were increased firstly and then decreased in deeper sediments. Their concentrations also peaked at around −0.3 cm with 206.31 μg L^{-1}, 26.42 μg L^{-1}, and 63.40 μg L^{-1}, respectively (Fig. 2L-N). Sulfide has similar distribution pattern with Co, Zn and Sb in vertical. But its concentration peak (113.53 μg L^{-1}) was observed in a deeper sediment and its peak range was wider (−0.8 cm to −1.4 cm) (Fig. 2H). Mn and Fe have the third distribution pattern with concentration increased in vertical (Fig. 2J-K). Despite Mn and Fe displayed a concentration peak at around −0.3 cm with 1.22 mg L^{-1} and 1.83 mg L^{-1}, respectively, their maximum concentrations appeared in deeper sediments. Consistent with 1D vertical profiles concentration peak, the 2D-HR images showed the enrichment of Fe, Co, and Sb were more elevated at −0.3 cm (Fig. 2k-l, n). Zn was more enriched above the depth of −1.0 cm in 2D-HR images (Fig. 2m). Besides, V was more concentrated above the SWI (Fig. 2i), whereas Mn and S were more enrichment Below the SWI (Fig. 2h-j). In horizontal direction, Fe, Co and Sb tended to concentrate in the left zone of 2D-HR images at −0.3 cm depth, while S, V, Mn, and Zn were more homogeneously distributed in 2D-HR images (Fig. 2h-n).

3.2. Distributions of dissolved TMs within microniches in sediments

Based on the distributions of 1D vertical profiles and 2D-HR images during aerobic periods (Fig. 2A-G and a-g), two sub-zones were selected to further decipher the biogeochemical processes of TMs in sediments. The first zone (zone 1) was located at around the −0.3 cm where several TMs co-peaked, and the second zone (zone 2) was located at around the 0.4 cm where a microniche was observed (Fig. 3A). To the right along the horizontal in zone 1 (−0.2 to −0.5 cm depth, Fig. 3A-B), the peak concentrations of Mn and Co were observed at about 2.0 mm from the left axis with 1.32 mg L^{-1} and 38.34 μg L^{-1}, respectively. In contrast, Fe and V showed the lowest concentrations (0.42 mg L^{-1} and 0.53 μg L^{-1}, respectively) at the same distance. Besides, concentration of Zn was continually increased and that of Sb was fluctuated slightly around 37.50 μg L^{-1}. In zone 2 (0.3 to 0.4 cm depth, Fig. 3A, C). The peak concentrations of V, Fe, Co, Zn, and Sb occurred at about 1.4 mm from the left axis, with 0.71 μg L^{-1}, 3.36 mg L^{-1}, 41.21 μg L^{-1}, 29.42 μg L^{-1}, and 84.30 μg L^{-1}, respectively. In contrast, Mn has a stable low concentration (0.28 mg L^{-1}) within a distance range of 0.6 to 2.2 mm from the left axis.

During hypoxic periods, zone 3 was also selected to investigate TMs biogeochemical processes (Fig. 4). The horizontal concentrations of TMs during hypoxic periods showed significantly different distribution patterns compared to that during aerobic periods. To the right along the horizontal, the peak concentrations of V and Co were observed at about 2.4 mm from the left axis with 0.62 μg L^{-1} and 3.13 mg L^{-1}, respectively. The concentration of Fe and Sb showed a decrease trend beginning at about 4.8 mm from the left axis (Fig. 4B). While Mn and Zn have a steady concentration distribution with 0.93 mg L^{-1} and 23.52 μg L^{-1}, respectively.

3.3. Correlations among TMs in different dimensions

Correlation analyses among TMs were further performed from different dimensions that was 1D vertical profiles from horizontally averaged 2D-HR images (1D—V, 0.5 to −3.2 cm depth), 1D horizontal transects (1D—H) from vertically averaged 2D-HR images, and the entire 2D-HR images (E2D). In the results of the horizontal correlation analyses (1D—H) in zone 1 during aerobic periods (Table 1A), the significant negative correlation ($r^2 = -0.71$, $p < 0.01$) between Fe and Co was same with that ($r^2 = -0.42$, $p < 0.01$) in 1D—V and in E2D ($r^2 = -0.53$, $p < 0.01$). In contrast, the results of the remaining four sets (Fe and V, Fe and Mn, Mn and V, Mn and Co) were completely changed even opposite compared with that in 1D—V. Similar differences were also observed in the correlation's comparison between E2D and the 1D—V.

For the correlation results of 1D—H in zone 3 during hypoxic periods (Table 1B), Fe exhibited a weak correlation both with Zn ($r^2 = 0.01$) and Mn ($r^2 = 0.18$), those results were corresponded with that in 1D—V and E2D indicated that Fe was decouple with Zn and Mn in sediments. In contrast, the weak correlations in 1D—V for the remained 3 set TMs [Fe and V ($r^2 = -0.06$), Fe and Co ($r^2 = -0.13$), Fe and Sb ($r^2 = -0.32$, $p < 0.01$)] were distinct different with the significant positive correlations ($r^2 \geq 0.31$, $p < 0.01$) both in 1D—H and E2D, suggested that the factor influenced the mobilization of V, Co, and Sb in vertical was definite different with that in horizontal.

4. Discussions

4.1. Vertical distributions of TMs record diagenesis

TMs distributions along sediment vertical profile can be used to record diagenesis which refer to a series biogeochemical processes occurred in different depth (Davison, 1993). Generally, intensive biogeochemical processes usually occurred follow the formation of a newly SWI in sediments especially with significant changes in oxygen conditions (Chen et al., 2018). Those biogeochemical processes could be considered as the early diagenesis, which mainly including the decomposition of organic matters (OM) (Bao et al., 2021; LaRowe et al., 2020), redox of Fe and/or Mn oxides (Bao et al., 2021; Davison, 1993), and microbiological metabolism (LaRowe et al., 2020; van de Velde et al., 2016). Obviously, those early diageneses usually occurred in the top few mm of surface sediments (Chen et al., 2018), which could facilitate the frequent electronic transfer and material exchange (Belzile et al., 1989; Chen et al., 2018; Davison et al., 1982). When several TMs concentrations were co-peaked at a certain depth in vertical profile, this indicating that intense biogeochemical processes may be occurred at this depth (Böning et al., 2015; Sochaczewski et al., 2008).

Herein, intensive biogeochemical processes in early diagenesis were

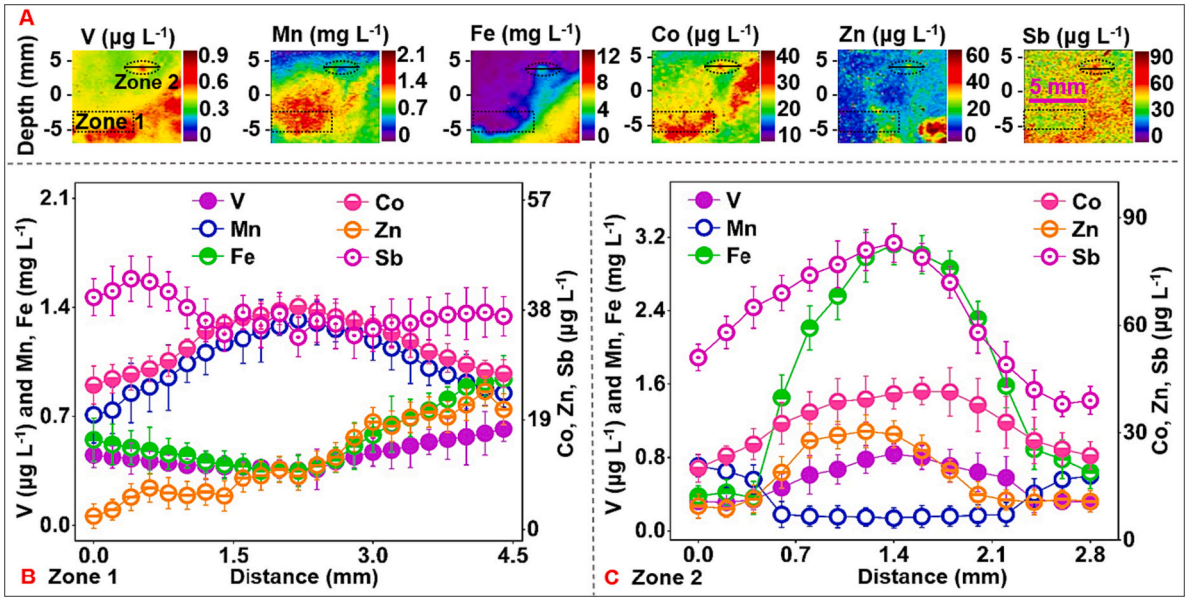

Fig. 3. Distribution of dissolved metals within microinches in sediments during aerobic periods. (A) Two selected zones (zone 1 and zone 2) near the sediment-water interface (SWI) from the 2D-HR images (Fig. 2b-g). Horizontal concentration distribution of V, Mn, Fe, Co, Zn, and Sb was collected from vertical averaged 2D in zone 1 (B) and zone 2 (C). The value of horizontal axis presents the distance from the left edge in selected zone, which was set as 0 mm.

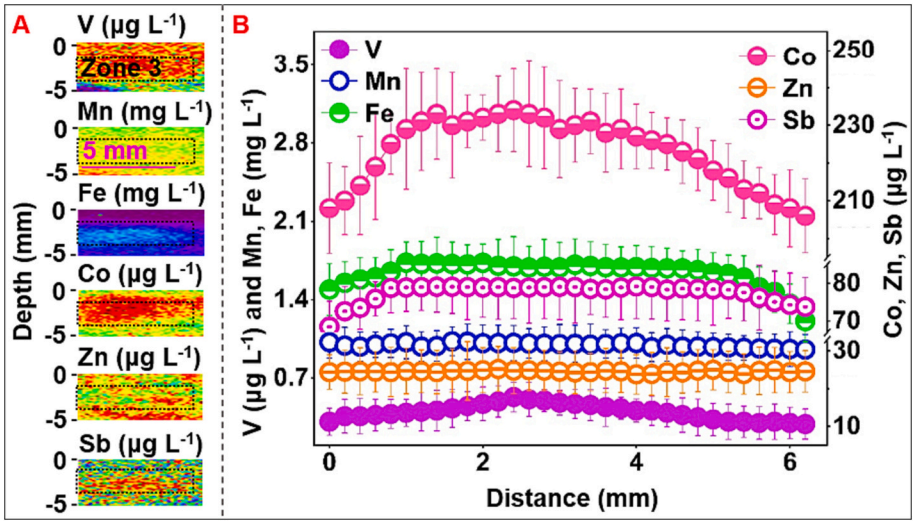

Fig. 4. Distributions of dissolved metals within microinches in sediments during hypoxic periods. (A) One selected zone near the sediment-water interface (SWI) from the 2D-HR images (Fig. 2i-n). (B) Horizontal concentration distribution of V, Mn, Fe, Co, Zn, and Sb was collected from vertical averaged 2D in zone 3. The value of horizontal axis presents the distance from the left edge in selected zone, which was set as 0 mm.

Table 1
Correlation analyses (r^2) between different elements during (A) aerobic and (B) hypoxic periods. (A) V, Mn, Fe, and Co in zone 1. 1D vertical profiles from horizontally averaged 2D images (1D—V, 0.5 to −3.2 cm depth, shown in Fig. 2B-E), 1D horizontal transects from vertically averaged 2D images (1D—H, shown in Fig. 3B), and the entire 2D image in zone 1 (E2D, shown in Fig. 3A). (B) Fe and other elements (V, Co, Zn, Sb, and Mn) in zone 3. 1D vertical profiles from horizontally averaged 2D images (1D—V, 0.5 to −3.2 cm depth, shown in Fig. 2I-N), 1D horizontal transects from vertically averaged 2D images (1D—H, shown in Fig. 4B), and the entire 2D image in zone 3 (E2D, shown in Fig. 4A). "*" indicates the significance level for $p < 0.01$, "−" indicates a negative correlation.

	1D-V	1D-H	E2D
A			
Fe & Co	−0.42*	−0.71*	−0.53*
Fe & V	0.03	0.78*	0.56*
Fe & Mn	0.12	−0.81*	−0.52*
Mn & V	0.32*	−0.73*	−0.41*
Mn & Co	−0.09	0.88*	0.59*
B			
Fe & V	−0.06	0.43*	0.31*
Fe & Co	−0.13	0.55*	0.38*
Fe & Zn	−0.10	0.01	−0.09
Fe & Sb	−0.32*	0.51*	0.34*
Fe & Mn	0.13	0.18	0.14

evidenced by the peak concentrations and enrichments of TMs near the SWI in 2D-HR images (Fig. 2). During aerobic periods, TMs (V, Mn, Co, Zn, and Sb) concentrations were co-peaked at around −0.3 cm, that was likely due to the decomposition of natural organic materials (NOM) in surface sediments (Bao et al., 2021; Sochaczewski et al., 2008; Wang et al., 2015). When NOM were decomposed in sediments, the first electron acceptors to be reduced in sediment vertical usually came from O_2, followed by nitrate, Mn(IV), Fe(III), and SO_4^{2-} (Och et al., 2012; Reimers et al., 2013; Su et al., 2019). As such, the intensive decomposition of NOM at −0.3 cm could lead the co-peak of TMs concentrations. Moreover, increasing of Fe concentration in vertical may result from enhancing reduction of Fe oxides with depth increasing (Fig. 2D; Chen et al., 2019; Tankere-Muller et al., 2007). Consistently, co-peak concentrations of V, Mn, Fe, Co, Zn and Sb were also observed at around −0.3 cm during hypoxic periods. Reductive dissolution of metal oxides may contribute to above co-peak of TMs concentrations due to the concentration of TMs in vertical profile during hypoxic periods (Fig. 2I-N) is overall higher than that during aerobic periods (Fig. 2B-G). Besides, significant higher concentrations (ranged from 40 to 118 μg L^{-1}) of S during hypoxic periods were observed compared with that (<6.00 μg L^{-1}) during aerobic periods (Fig. 2A, a), which was likely due to intensive metabolism of sulfate-reducing bacteria in surface sediments (Motelica-Heino et al., 2003; Su et al., 2019). Collectively, those results collectively suggested that intensive biogeochemical processes usually occurred within early diagenesis in surface sediments.

In deeper sediments, biogeochemical processes are generally weaker due to the properties of sediments have stabilized after the modification by the intensive biogeochemical processes in the original surface sediments (Chen et al., 2018; Davison, 1993). Naturally, the original surface sediments must grow to be the deeper sediments with the continuous coverage of new particulate matters. Correspondingly, the biogeochemical processes also changed from being intense in original surface sediments to being weak in deeper sediments (Belzile et al., 1989; Davison, 1993). The biogeochemical processes in deeper sediments commonly including the reduction of metals oxides (Bao et al., 2021; Davison, 1993), mineralization and co-precipitation (Och et al., 2012; Shaw et al., 1990), and the dissolution of acid-sensitive metal sulfides or carbonates (Malkin et al., 2014; van de Velde et al., 2016). Herein, the relative low concentration of TMs (V, Co, Zn, and Sb) in deeper sediments (below −2.7 cm) were observed in both aerobic and hypoxic periods (Fig. 2), indicated weak biogeochemical processes in deeper sediments. Despite the concentration of Fe and Mn showed a high value in the depth range from −2.7 cm to −3.2 cm, the low concentrations in deeper sediments (below −6.5 cm) have been documented in previous work (Chen et al., 2019; Wang et al., 2015) also demonstrated the weak biogeochemical processes in deep sediments.

In short, above discussions indicate that the biogeochemical processes of TMs commonly vary at different depth with the continuous coverage of new particulate matters, and the distributions of TMs along sediment vertical profile record the biogeochemical processes of TMs at different sedimentation historical.

4.2. Distributions of TMs within microniches in horizontal reflect mobilization

Previous studies to investigate the mobilization of TMs in sediments were mainly based on the distributions and correlation analyses in vertical profile (Jin et al., 2019; Smith et al., 2011; Zhou et al., 2018). However, the comparison of TMs mobilization between vertical profiles

and microniches was usually overlooked, especially the underlying biogeochemical processes of those differences were poorly understood (Tessier et al., 1996; Zhou et al., 2018, 2020).

In contrast to distributions of TMs along sediment vertical, TMs distributions within microniches in horizontal virtually reflect their mobilization processes. In zone 1, correlations of Fe and Co in ID-H were significant negative correlations ($r^2 = -0.71$, $p < 0.01$) indicated that their mobilization were mutually exclusive (Fig. 3B, Table 1A). This was evidenced by the high enrichment of Co and contrast low enrichment of Fe from 2D-HR images in depth range from 5 to −5 mm (Fig. 3A). Consistent with our result, the mutually exclusive mobilization between Fe and Co was reported in Belgian coastal zone in the North Sea (Zhou et al., 2020). Those results indicated that the mutually exclusive mobilization of Fe and Co was likely existed in aquatic sediments. Besides, while correlations of Mn and Co concentrations in 1D—V were weak ($r^2 = -0.09$, $p > 0.05$), significant positive correlation were observed in 1D—H and E2D (Table 1A). The coincident enrichment zone of Mn and Co in 2D-HR images in depth range from 5 to −5 mm further evidenced that mobilization of Co was associate with Mn (Fig. 3A). Obviously, the couple mobilization of Mn and Co couldn't be detected if solely rely on vertical data ($r^2 = -0.09$, $p > 0.05$; Table 1A). Similarly, the weak correlations ($r^2 = 0.03$, $p > 0.05$) between Fe and V in 1D—V suggested that their mobilization was also decoupled. However, the coincident enrichment of V and Fe from 2D-HR images in the depth range from 5 to −5 mm indicated that V mobilization was closely associated with Fe (Fig. 3A). Obviously, the result for the mobilization of V was closely associated with Mn relied solely on the significant positive correlation in 1D—V was mistake ($r^2 = 0.32$, $p < 0.01$; Table 1A). Also, the correlation results in 1D—V for the remain two sets (Fe and Mn, Mn and V) were completely different even opposite compared with that in 1D—H and E2D (Table 1A). Collectively, those above discussions implied that 2D-HR data can offer an update complement to 1D data for further understand the biogeochemical processes of TMs in sediments.

Additionally, in zone 3, the mobilization of V, Co, and Sb were associated with Fe was evidenced by the significant positive correlations in 1D—H and their overlapping enrichment in 2D-HR images (Fig. 4B, Table 1B). Regrettably, bias would be also brought in understanding the mobilization of V, Co, and Sb with Fe if solely relied on their weak or negative correlations in 1D—V (Table 1B). For Zn and Mn, their discrete enrichment with Fe in 2D-HR images implied their mobilization were decouple with Fe, those results were consistent with the correlation results in 1D—V (Fig. 4B, Table 1B). As such, spatial distributions of TMs within microniches in horizontal at specific depth were favored to illustrate the regional mobilization processes occurred at the same time/historical. Herein, both the couple mobilization of Mn and Co, Fe and V in zone 1 were evidenced by their coincident enrichment from 2D-HR Images (Fig. 3A-B). Besides, discrete and small-scale (mm to μm) TMs mobilization resulted in peak concentrations in microniches (Fig. 3A, C). Especially in zone 2, a microniches above the SWI, the coincident enrichment region indicated that the mobilization of V, Co, Zn, Sb were likely to associate with Fe not Mn (Fig. 3A, C, and S3). Coincident with our results, the existence of microniches were observed in Gotland basin sediment in the Baltic Sea (Zhou et al., 2020). Those results suggested that microniches mobilization are prevalent in aquatic ecosystem sediments. Unfortunately, mobilization of TMs in these microniches could not detected from 1D—V data (Ho et al., 2007).

Taken together, the correlations in 1D—V were usually different with that in 1D—H and E2D, suggesting that using 1D—V information to illustrate TMs mobilization in sediment may bring bias even incorrect understanding (Fig. 2, Table 1). Because every single data in 1D—V was the averaged concentration for the micro rectangle piece of zone in vertical profiles. Besides, the mobilization of TMs is usually occurred in discrete, and micro-scale locations (microniches) (Bao et al., 2021; Zhou et al., 2020). For better and further understanding of the mobilization of TMs in sediments, 2D-HR data is an update complement to 1D data.

4.3. Understanding the biogeochemical process patterns of TMs in sediments

A complete biogeochemical process patterns of TMs in sediments was constructed by the diagenesis in vertical and mobilization within microniches in horizontal. Surface runoff, particulate matter and NOM residues carrying TMs from the watershed continue flowed into the freshwater ecosystems, resulted in the accumulation of TMs in sediments (Chen et al., 2019; Maavara et al., 2020; Wang et al., 2015). In the early diagenesis, intense biogeochemical processes usually lead to high concentrations of TMs in surface sediments (Fig. 2; Chen et al., 2018; Zhou et al., 2020). In contrast, after experiencing the modification of intensive biogeochemical processes during the early diagenesis, a weaker biogeochemical process was likely occurred in late diagenesis (Fig. 2; Chen et al., 2018). Additionally, in the horizontal direction, variations of microenvironmental conditions (e.g., dissolved oxygen, degradation of NOM, microbial populations) could lead to the changes of mobilization mechanisms (pathways) of TMs (Figs. 3 and 4; Zhou et al., 2020). This is the reason for the significant spatial heterogeneity in sediments. Taken together, horizontal microniches distributions of TMs at specific depth reflected their mobilization processes in corresponding depth, the superposition of mobilization processes in horizontal at different depths constructed the vertical diagenesis in sediments.

5. Conclusions

2D-HR distributions of TMs in sediments were detected by LA-ICP-MS. These results were normally overlooked by the traditional ex-situ sampling due to their data were averaged in its resolution regional. Because the interpretations of TMs mobilization in 1D—V are usually different even opposite with that in 1D—H and E2D, bias even misinterpretations maybe be brought if the interpretations for TMs mobilization are solely relied on 1D—V data. Based on the 2D-HR data, the patterns of TMs biogeochemical processes occur in sediments were interpreted as: 1) microniches distributions of TMs in horizontal at specific depth reflected their mobilization processes within microenvironments; 2) then the superposition of mobilization processes in horizontal at different depths constructed the vertical diagenesis in sediments. Our findings showed that 2D-HR data can offer an update complement to 1D data for further understanding the biogeochemical processes of TMs in sediments. Further progress on understanding the biogeochemical processes of TMs can be made by deciphering the detail information in vertical and horizontal with the combination of traditional measurement methods and advance 2D-HR analyses.

CRediT authorship contribution statement

Quan Chen: Data curation, Formal analysis, Investigation, Writing – original draft. **Shu Xu:** Data curation, Investigation. **Jingfu Wang:** Conceptualization, Supervision, Funding acquisition, Writing – review & editing. **Dengjun Wang:** Writing – review & editing. **Zhihui Dai:** Data curation, Methodology. **Peng Liao:** Writing – review & editing. **Jiao-Jiao Yang:** Data curation. **Wen Guo:** Data curation. **Shiming Ding:** Writing – review & editing. **Jingan Chen:** Conceptualization, Supervision, Funding acquisition.

Declaration of competing interest

The authors declare that they have no known competing financial interests or personal relationships that could have appeared to influence the work reported in this paper.

Data availability

No data was used for the research described in the article.

Acknowledgments

This study was sponsored by the Strategic Priority Research Program of CAS (No. XDB40020400), National Key Research and Development Program of China, the Science and Technology Service Plan of CAS (KFJSTSQYZD202124001), the Central Leading Local Science and Technology Development Fund Project (20214028), the Chinese NSF project (No. 41773145, 41977296, 42077313, 42273083), and the Youth Innovation Promotion Association CAS (No. 2019389).

Appendix A. Supplementary data

Supplementary data to this article can be found online at https://doi.org/10.1016/j.scitotenv.2023.166404.

References

Bao, Y., Bolan, N.S., Lai, J., Wang, Y., Jin, X., Kirkham, M.B., Wu, X., Fang, Z., Zhang, Y., Wang, H., 2021. Interactions between organic matter and Fe (hydr)oxides and their influences on immobilization and remobilization of metal(loid)s: a review. Crit. Rev. Environ. Sci. Technol. 52 (22), 4016–4037.

Belzile, N., Vitre, R.R.D., Tessier, A., 1989. In situ collection of diagenetic iron and manganese oxyhydroxides from natural sediments. Nature 340 (6232), 376–377.

Böning, P., Shaw, T., Pahnke, K., Brumsack, H.-J., 2015. Nickel as indicator of fresh organic matter in upwelling sediments. Geochim. Cosmochim. Acta 162, 99–108.

Chen, J., Wang, J., Guo, J., Yu, J., Zeng, Y., Yang, H., Zhang, R., 2018. Eco-environment of reservoirs in China. Prog. Phys. Geogr. 42 (2), 185–201.

Chen, Q., Chen, J.A., Wang, J.F., Guo, J.Y., Jin, Z.X., Yu, P.P., Ma, Z.Z., 2019. In situ, high-resolution evidence of phosphorus release from sediments controlled by the reductive dissolution of iron-bound phosphorus in a deep reservoir, southwestern China. Sci. Total Environ. 666, 39–45.

Davison, W., 1993. Iron and manganese in lakes. Earth-Sci. Rev. 34, 119–163.

Davison, W., Zhang, H., 1994. In situ speciation measurements of trace components in natural waters using thin-film gels. Nature 367 (6463), 546–548.

Davison, W., Woof, C., Rigg, E., 1982. The dynamics of iron and manganese in a seasonally anoxic lake; direct measurement of fluxes using sediment traps. Limnol. Oceanogr. 27 (6), 987–1003.

Ding, S.M., Wang, Y., Zhang, L., Xu, L., Gong, M., Zhang, C.S., 2016. New holder configurations for use in the diffusive gradients in thin films (DGT) technique. RSC Adv. 6 (91), 88143–88156.

Ernstberger, H., Davison, W., Zhang, H., Tye, A., Young, S., 2002. Measurement and dynamic modeling of trace metal mobilization in soils using DGT and DIFS. Environ. Sci. Technol. 36 (3), 349–354.

Fan, X., Ding, S., Chen, M., Gao, S., Fu, Z., Gong, M., Tsang, D.C.W., Wang, Y., Zhang, C., 2019. Peak chromium pollution in summer and winter caused by high mobility of chromium in sediment of a eutrophic lake: in situ evidence from high spatiotemporal sampling. Environ. Sci. Technol. 53 (9), 4755–4764.

Gao, L., Gao, B., Zhou, H., Xu, D., Wang, Q., Yin, S., 2016. Assessing the remobilization of antimony in sediments by DGT: a case study in a tributary of the three gorges reservoir. Environ. Pollut. 214, 600–607.

Gao, Y., van de Velde, S., Williams, P.N., Baeyens, W., Zhang, H., 2015. Two dimensional images of dissolved sulphide and metals in anoxic sediments by a novel DGT probe and optical scanning techniques. TrAC Trends Anal. Chem. 66, 63–71.

Grill, G., Lehner, B., Thieme, M., Geenen, B., Tickner, D., Antonelli, F., Babu, S., Borrelli, P., Cheng, L., Crochetiere, H., Ehalt Macedo, H., Filgueiras, R., Goichot, M., Higgins, J., Hogan, Z., Lip, B., McClain, M.E., Meng, J., Mulligan, M., Nilsson, C., Olden, J.D., Opperman, J.J., Petry, P., Reidy Liermann, C., Sáenz, L., Salinas-Rodríguez, S., Schelle, P., Schmitt, R.J.P., Snider, J., Tan, F., Tockner, K., Valdujo, P. H., van Soesbergen, A., Zarfl, C., 2019. Mapping the world's free-flowing rivers. Nature 569 (7755), 215–221.

Hamilton-Taylor, J., Smith, E.J., Davison, W., Sugiyama, M., 2005. Resolving and modeling the effects of Fe and Mn redox cycling on trace metal behavior in a seasonally anoxic lake. Geochim. Cosmochim. Acta 69 (8), 1947–1960.

Hammond, N.W., Birgand, F., Carey, C.C., Bookout, B., Breef-Pilz, A., Schreiber, M.E., 2023. High-frequency sensor data capture short-term variability in Fe and Mn concentrations due to hypolimnetic oxygenation and seasonal dynamics in a drinking water reservoir. Water Res. 240, 120084.

Ho, T.Y., Wen, L.S., You, C.F., Lee, D.C., 2007. The trace-metal composition of size-fractionated plankton in the South China Sea: biotic versus abiotic sources. Limnol. Oceanogr. 52 (5), 1776–1788.

Jin, Z., Ding, S., Sun, Q., Gao, S., Fu, Z., Gong, M., Lin, J., Wang, D., Wang, Y., 2019. High resolution spatiotemporal sampling as a tool for comprehensive assessment of zinc mobility and pollution in sediments of a eutrophic lake. J. Hazard. Mater. 364, 182–191.

LaRowe, D.E., Arndt, S., Bradley, J.A., Burwicz, E., Dale, A.W., Amend, J.P., 2020. Organic carbon and microbial activity in marine sediments on a global scale throughout the quaternary. Geochim. Cosmochim. Acta 286, 227–247.

Lehto, N.J., Davison, W., Zhang, H., 2012. The use of ultra-thin diffusive gradients in thin-films (DGT) devices for the analysis of trace metal dynamics in soils and sediments: a measurement and modelling approach. Environ. Chem. 9 (4), 415–423.

Li, C., Ding, S., Yang, L., Zhu, Q., Chen, M., Tsang, D.C.W., Cai, G., Feng, C., Wang, Y., Zhang, C., 2019. Planar optode: a two-dimensional imaging technique for studying spatial-temporal dynamics of solutes in sediment and soil. Earth-Sci. Rev. 197, 102916.

Liu, M., He, Y., Baumann, Z., Zhang, Q., Jing, X., Mason, R.P., Xie, H., Shen, H., Chen, L., Zhang, W., Zhang, Q., Wang, X., 2020. The impact of the three gorges dam on the fate of metal contaminants across the river-ocean continuum. Water Res. 185, 116295.

Luders, K., Dahmke, A., Fiedler, M., Kober, R., 2020. Temperature influence on mobilisation and (re)fixation of trace elements and heavy metals in column tests with aquifer sediments from 10 to 70 degrees C. Water Res. 169, 115266.

Luther, G.W., Brendel, P.J., Lewis, B.L., Sundby, B., Lefrançois, L., Silverberg, N., Nuzzio, D.B., 1998. Simultaneous measurement of O-2, Mn, Fe, I-, and S(-II) in marine pore waters with a solid-state voltammetric microelectrode. Limnol. Oceanogr. 43 (2), 325–333.

Maavara, T., Chen, Q., Van Meter, K., Brown, L.E., Zhang, J., Ni, J., Zarfl, C., 2020. River dam impacts on biogeochemical cycling. Nat. Rev. Earth Environ. 1 (2), 103–116.

Malkin, S.Y., Rao, A.M.F., Seitaj, D., Vasquez-Cardenas, D., Zetsche, E.-M., Hidalgo-Martinez, S., Boschker, H.T.S., Meysman, F.J.R., 2014. Erratum: natural occurrence of microbial sulphur oxidation by long-range electron transport in the seafloor. ISME. J. 8 (9), 1843–1854.

Motelica-Heino, M., Naylor, C., Zhang, H., Davison, W., 2003. Simultaneous release of metals and sulfide in lacustrine sediment. Environ. Sci. Technol. 37 (19), 4374–4381.

Och, L.M., Müller, B., Voegelin, A., Ulrich, A., Göttlicher, J., Steiniger, R., Mangold, S., Vologina, E.G., Sturm, M., 2012. New insights into the formation and burial of Fe/Mn accumulations in Lake Baikal sediments. Chem. Geol. 330, 244–259.

Peijnenburg, W.J.G.M., Teasdale, P.R., Reible, D., Mondon, J., Bennett, W.W., Campbell, P.G.C., 2014. Passive sampling methods for contaminated sediments: state of the science for metals. Integr. Environ. Assess. 10 (2), 179–196.

Reimers, C.E., Alleau, Y., Bauer, J.E., Delaney, J., Girguis, P.R., Schrader, P.S., Stecher, H.A., 2013. Redox effects on the microbial degradation of refractory organic matter in marine sediments. Geochim. Cosmochim. Acta 121, 582–598.

Ren, M., Ding, S., Dai, Z., Wang, J., Li, C., Zhong, Z., Cao, J., Yang, L., Tsang, D.C.W., Xu, S., Yang, C., Wang, Y., 2021. A new DGT technique comprising a hybrid sensor for the simultaneous high resolution 2-D imaging of sulfides, metallic cations, oxyanions and dissolved oxygen. J. Hazard. Mater. 403, 123597.

Rodriguez, A.B., McKee, B.A., Miller, C.B., Bost, M.C., Atencio, A.N., 2020. Coastal sedimentation across North America doubled in the 20(th) century despite river dams. Nat. Commun. 11 (1), 3249.

Schroth, A.W., Giles, C.D., Isles, P.D., Xu, Y., Perzan, Z., Druschel, G.K., 2015. Dynamic coupling of iron, manganese, and phosphorus behavior in water and sediment of shallow ice-covered eutrophic lakes. Environ. Sci. Technol. 49 (16), 9758–9767.

Shaw, T.J., Gieskes, J.M., Jahnke, R.A., 1990. Early diagenesis in differing depositional environments: the response of transition metals in pore water. Geochim. Cosmochim. Acta 54 (5), 1233–1246.

Smith, L., Watzin, M.C., Druschel, G., 2011. Relating sediment phosphorus mobility to seasonal and diel redox fluctuations at the sediment-water interface in a eutrophic freshwater lake. Limnol. Oceanogr. 56 (6), 2251–2264.

Sochaczewski, Ł., Stockdale, A., Davison, W., Tych, W., Zhang, H., 2008. A three-dimensional reactive transport model for sediments, incorporating microniches. Environ. Chem. 5 (3), 218–225.

Stockdale, A., Davison, W., Zhang, H., 2009. Micro-scale biogeochemical heterogeneity in sediments: a review of available technology and observed evidence. Earth-Sci. Rev. 92 (1–2), 81–97.

Su, G., Zopfi, J., Yao, H., Steinle, L., Niemann, H., Lehmann, M.F., 2019. Manganese/iron-supported sulfate-dependent anaerobic oxidation of methane by archaea in lake sediments. Limnol. Oceanogr. 65 (4), 863–875.

Tankere-Muller, S., Zhang, H., Davison, W., Finke, N., Larsen, O., Stahl, H., Glud, R.N., 2007. Fine scale remobilisation of Fe, Mn, Co, Ni, Cu and Cd in contaminated marine sediment. Mar. Chem. 106 (1–2), 192–207.

Tessier, A., Fortin, D., Belzile, N., DeVitre, R.R., Leppard, G.G., 1996. Metal sorption to diagenetic iron and manganese oxyhydroxides and associated organic matter: narrowing the gap between field and laboratory measurements. Geochim. Cosmochim. Acta 60 (3), 387–404.

van de Velde, S., Lesven, L., Burdorf, L.D.W., Hidalgo-Martinez, S., Geelhoed, J.S., Van Rijswijk, P., Gao, Y., Meysman, F.J.R., 2016. The impact of electrogenic sulfur oxidation on the biogeochemistry of coastal sediments: a field study. Geochim. Cosmochim. Acta 194, 211–232.

Wang, G., A, Y., Jiang, H., Fu, Q., Zheng, B., 2015. Modeling the source contribution of heavy metals in surficial sediment and analysis of their historical changes in the vertical sediments of a drinking water reservoir. J. Hydrol. 520, 37–51.

Wang, Y., Ding, S.M., Shi, L., Gong, M., Xu, S., Zhang, C.S., 2017. Simultaneous measurements of cations and anions using diffusive gradients in thin films with a ZrO-Chelex mixed binding layer. Anal. Chim. Acta 972, 1–11.

Xue, S., Jian, H., Yang, F., Liu, Q., Yao, Q., 2022. Impact of water-sediment regulation on the concentration and transport of dissolved heavy metals in the middle and lower reaches of the Yellow River. Sci. Total Environ. 806, 150535.

Zhang, C., Ding, S., Xu, D., Tang, Y., Wong, M.H., 2014. Bioavailability assessment of phosphorus and metals in soils and sediments: a review of diffusive gradients in thin films (DGT). Environ. Monit. Assess. 186 (11), 7367–7378.

Zhou, C., van de Velde, S., Baeyens, W., Gao, Y., 2018. Comparison of Chelex based resins in diffusive gradients in thin-film for high resolution assessment of metals. Talanta 186, 397–405.

Zhou, C., Gao, Y., Gaulier, C., Luo, M., Zhang, X., Bratkic, A., Davison, W., Baeyens, W., 2020. Advances in understanding mobilization processes of trace metals in marine sediments. Environ. Sci. Technol. 54 (23), 15151–15161.
Zhu, H., Bing, H., Wu, Y., Zhou, J., Sun, H., Wang, J., Wang, X., 2019. The spatial and vertical distribution of heavy metal contamination in sediments of the three gorges reservoir determined by anti-seasonal flow regulation. Sci. Total Environ. 664, 79–88.
Zhu, J.Y., Song, C.Q., Wang, J.D., Ke, L.H., 2020. China's inland water dynamics: the significance of water body types. Proc. Natl. Acad. Sci. U. S. A. 117 (25), 13876–13878.
Zhu, Q., Aller, R.C., Fan, Y., 2006. Two-dimensional pH distributions and dynamics in bioturbated marine sediments. Geochim. Cosmochim. Acta 70 (19), 4933–4949.